

# Leveraging Local Planar Motion Property for Robust Visual Matching and Localization

Yanmei Jiao, Qunkang Zhang, Bo Fu, Fuzhang Han, Yue Wang, and Rong Xiong

**Abstract**—One primary difficulty preventing the visual localization for service robots is the robustness against changes, including environmental changes and perspective changes. In recent years, learning-based feature matching methods have been widely studied and effectively verified in practical applications. Learning-based feature matching effectively solves the problem of environmental changes, including illumination changes and man-made changes. However, there is still room for improvement dealing with large perspective changes. In this paper, we leverage local planar motion property to simplify the affine transform and propose an augmentation-based feature matching method that greatly enhances the robustness to perspective changes. The proposed feature matching approach maintains low matching costs as the augmentation is performed on the simplified affine matrix space. Combined with the motion property aided minimal solution for pose estimation, an end-to-end robust visual localization system is proposed which is shown to bring 67% improvement in localization performance under large perspective changes in publicly available OpenLORIS dataset, while increasing computational cost by only 20% by using batch processing techniques with a single GPU. In addition, a guide for map frame selection is presented to support robust localization with very sparse map frames in storage. Experiments on the classified dataset with environmental changes and perspective changes validate the effectiveness of the proposed system.

## I. INTRODUCTION

The last decade has witnessed a fast-growing volume of service robots applied in various indoor scenarios e.g. bank lobby, restaurant, and home. One of the fundamental techniques for these robots is localization [1], [2]. To further save the cost of robots, vision based localization becomes a popular solution [3], [4], which is widely studied and relatively mature for autonomous vehicles [5]–[7]. However, compared with autonomous vehicles, the localization for service robots has two additional difficulties. Firstly, when dealing with *environmental changes* (EC), we can not assume semantic features to be known as autonomous driving, so only low-level point-based features can be utilized. However, the point features are sensitive to long-term EC, such as illumination variations due to complex lighting conditions (including natural and artificial lighting) in the room, and changes and occlusion of objects due to frequent human activities in the indoor environment. Secondly, the *perspective changes* (PC) introduced by camera motion is more

Yanmei Jiao, Qunkang Zhang, Bo Fu, Fuzhang Han, Yue Wang and Rong Xiong are with the State Key Laboratory of Industrial Control and Technology, Zhejiang University, Hangzhou, China, and with the Institute of Cyber-Systems and Control, Zhejiang University, Hangzhou, China. (Corresponding author: Yue Wang, Email: wangyue@ipc.zju.edu.cn). This letter has Appendix available at <https://github.com/slinkle/Divided-Openloris>.

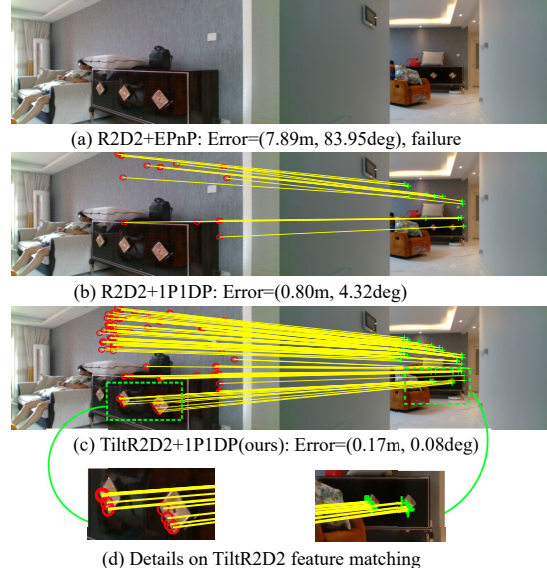


Fig. 1. Comparison of the localization performance in the same indoor scene. Each caption below subfigures (a)–(c) indicates the feature matching method and the subsequent pose estimation method, as well as the localization error of the estimated pose. Specifically, R2D2 [10] is a learning-based feature extraction method and TiltR2D2 is the proposed augmentation-based feature matching method. EPnP [11] and 1P1DP [12] are minimal solutions which estimate the camera pose using 2D–3D feature matches. The yellow lines between two images are inliers found by the corresponding pose estimation algorithm among all correspondences matched by different features. The proposed TiltR2D2 matches a large number of inliers under large perspective changes, which assists the subsequent pose estimation algorithm to achieve better localization accuracy.

serious than in outdoors, as the distance between robot and scene is shorter, where small turns of the robot can lead to large changes in image appearance. In addition, indoor service robot's route is not constrained by lanes. The turn of service robot is thus free, and larger PC will exist. The difficulty in maintaining the robustness of large PC lies in the small overlap area between images and the existence of deformation. Therefore, not only the outlier rate in feature matches is high, but also the number of matches is small.

To cope with EC, many learning-based features are proposed which are trained on a large number of images with various variations, resulting in strong robustness to environmental variations [8]. However relying on the learning-based approaches to improve invariance to PC by augmenting the training set is difficult, as demonstrated in experiments in previous study [9].

An intuitive idea to eliminate the effect of large viewpoint variation is to enrich feature matches by further augmenting query image with affine transform [13]. The augmentation

brings more feature matches, consequently more inliers. Unfortunately, at the same time, since feature matching has to be performed on multiple augmented images, the augmentation is expensive both in time and hardware, and may lead to higher outlier rate.

In this paper, we combine the learning-based feature with classic image augmentation strategy to overcome the large PC and leverage the local planar motion property to address the two challenges. For efficiency, we introduce motion property to simplify affine transform, leading to reduced dimensions of augmentation and smaller matching costs. In addition, we leverage the robustness to perspective changes obtained by the proposed method to explore the map frame selection guide, which can support the localization with very sparse map frames in storage, satisfying the service robots hardware requirement. For picking inliers, we use the minimal solution proposed in our previous work which models the reduced subspace to consider both features with and without depth, to enable robust pose estimation in features with a high percentage of outliers [12]. Based on the above two points, we propose a simple-yet-effective robust visual localization system for service robots. Comparison of localization performance shown in Fig. 1 demonstrates that the proposed localization system can obtain more inliers and achieve better localization accuracy under large perspective changes. In experiments, we manually divide data in the dimension of PC and EC, to study the effect of PC on localization performance of service robot firstly, and secondly compare with other methods in finer granularity. Results show that the proposed system is effective for both PC and EC, with a significant improvement for PC. In summary, the contributions of this work are listed as follows:

- An experimental evaluation of existing learning-based feature matching methods in the face of EC and PC is presented, which points out that the main challenge that current indoor localization should target is the invariance to large PC.
- A theoretical analysis of feature matching is derived which explicitly models motion property into front-end and thus an efficient augmentation-based feature matching method is proposed to deal with large PC.
- A simple map selection guide is explored which can support the localization with very sparse frames in storage, satisfying the service robots hardware requirement.
- The source code is available on github<sup>1</sup>, which is a contribution to the community for comparative study.

## II. RELATED WORKS

### A. Visual localization

Traditionally, there are two lines of visual localization approaches. The first is the image retrieval based localization, which can also be called place recognition based methods. The pose of query image is approximated by the pose of top-retrieved database images using the image-based

representations for indexing [14], [15]. The second is 3D model based approaches, which solve the camera pose using matched feature correspondences between query image and pre-built 3D map [16], [17], leading to much higher accuracy. However, the performance will degenerate significantly facing serious changes in environment with a high outlier rate in feature correspondences. Recently, the hierarchical localization framework is widely used which converges the two lines of methods by using place recognition to reduce the local region and feature based localization for accurate pose estimation [5]. The idea of incorporating higher-level scene understanding into visual localization for autonomous vehicles has attracted more attention in recent years. The semantic features extracted on informative regions (such as sky, building, vegetation, road and pole) are integrated to enhance the feature matching robustness [18] or pose refinement [19].

### B. Motion property for localization

The outliers are unavoidable in feature matches provided by the front-end, which need to be rejected by the robust pose estimation algorithm in the back-end. The typical way to achieve robust estimation is random sample consensus (RANSAC) [20]. To enhance the robustness of RANSAC, many efforts have been made to reduce the minimum number of feature correspondences for pose estimation by leveraging motion property. One type of motion property is the measurement of pitch and roll angles of a robot obtained by gravity direction alignment from inertial measurements. With the known pitch and roll angles, the minimal solutions using two points are presented in [7], [21]. Another type of motion property is planar motion which is commonly used in indoor localization. In [22], the minimal solution using only a single affine correspondence is derived under planar motion. In our previous work, the minimal solution using one point correspondence with depth and another one without depth for locally planar moving robots is shown to achieve more robust performance that can deal with up to 80% outlier rate. However, the performance of robust visual localization is still limited by the absolute number of inliers, even when outlier removal is perfect [23].

### C. Visual matching

For robust visual matching, learning-based features [8] are shown to outperform conventional hand-crafted methods, like SIFT [24] and ORB [25], in presence of environmental variations. To generate more matches, NCNet [26] builds a dense volume encoding per-pixel similarity between two images, which enables a dense feature matches after learning. However, when dealing with large perspective changes, the performance of learning-based methods is significantly reduced due to the small overlap and deformation [9]. To obtain more inliers when large perspective changes exist, ASIFT [13] is the first to achieve full affine invariance by simulating all affine parameters for augmentation. However, it requires a considerable number of image augmentation, which is time-

<sup>1</sup>The Appendix together with the source code can be found in <https://github.com/slinkle/Divided-Openloris>

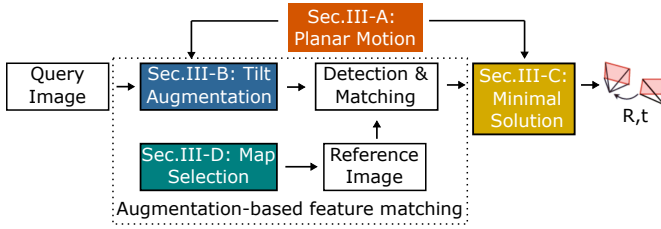


Fig. 2. The framework of the proposed local planar motion aided robust visual localization system.

consuming and difficult to meet the requirement of robot applications in natural scene localization.

### III. MOTION PROPERTY AIDED LOCALIZATION SYSTEM

In this paper, we leverage the local planar motion property of wheeled mobile robots to increase the robustness of both feature matching and pose estimation, thus improving the end-to-end system performance of the visual localization. For the feature matching at the front-end, we simplify the affine distortion matrix with the motion property and propose a tilt augmentation strategy to suppress the variation caused by PC. Combined with the learning-based feature extraction, the proposed technique can increase a considerable number of matching inliers, as illustrated in Fig.1. For the pose estimation at the back-end, we use the minimal solution in our previous work [12] utilizing either map feature points with depth or ones without depth, thus taking full advantage of all correspondences. The framework of the proposed motion property aided visual localization system is shown in Fig. 2. Taking one query image as input, the augmentation-based feature matching is first applied to obtain matches, and the pose estimation algorithm is then performed in the RANSAC framework to solve the camera pose. In the following, we first introduce the local planar motion property in indoor visual localization.

#### A. Local planar motion property

Service robots generally move on planar surfaces, or at least locally planar surfaces. For local planar motion shown in Fig. 3 (a), with the assumption that the camera plane is perpendicular to the ground, the pose from the coordinate system of reference view  $r$  to query view  $q$  can be expressed as

$$\mathbf{R} = \begin{bmatrix} \cos \theta & 0 & \sin \theta \\ 0 & 1 & 0 \\ -\sin \theta & 0 & \cos \theta \end{bmatrix}, \mathbf{t} = \begin{bmatrix} t_x \\ 0 \\ t_z \end{bmatrix} \quad (1)$$

where  $\theta$  denotes the rotation angle around axis  $y$  and  $t_x, t_z$  denotes the translation along axis  $x$  and  $z$ . Note that the assumption can be easily satisfied by rotating the appropriate pitch and roll angles to construct a virtual camera coordinate system of which the image plane is perpendicular to the ground, and the corresponding angles can be obtained from extrinsic calibration. Some details are shown in Appendix A<sup>1</sup>.

Therefore the DoF of the transformation matrix under local planar motion is reduced. Leveraging this property, the problem of indoor visual localization can be mathematically relaxed, and both the feature matching in the front-end and

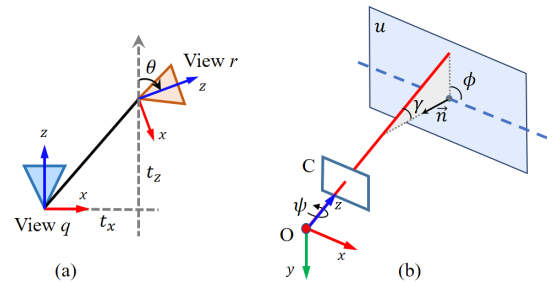


Fig. 3. (a) The illustration of local planar motion between query and reference views. (b) The geometric interpretation of affine decomposition of one camera facing one vertical object plane.

pose estimation in the back-end can be simplified. Specifically, in the front-end, to address the difficulty of feature matching caused by viewpoint difference due to camera motion, we reformulate the affine matrix by combining the local planar motion characteristics, so as to achieve full affine invariance, as detailed in the next subsection.

#### B. Augmentation based feature matching

**Affine model in local planar motion:** According to the camera imaging principle, the viewpoint variance between two images can be formulated by projective deformation, which can be locally simplified to affine distortion if the subject is a smooth plane. Since the feature points in the indoor environment are mainly distributed on vertical walls, we next consider the affine model in detail. According to the affine theorem proposed in [13], any affine map  $\mathbf{A}$  has a unique decomposition

$$\mathbf{A} = \lambda \begin{bmatrix} \cos \psi & -\sin \psi \\ \sin \psi & \cos \psi \end{bmatrix} \begin{bmatrix} \tau & 0 \\ 0 & 1 \end{bmatrix} \begin{bmatrix} \cos \phi & -\sin \phi \\ \sin \phi & \cos \phi \end{bmatrix} \quad (2)$$

where  $\lambda > 0$ ,  $\psi \in [0, 2\pi)$ ,  $\phi \in [0, \pi)$ , and  $\tau > 1$ . And  $\phi$  is called longitude angle which is the angle between the plane containing the normal vector  $\vec{n}$  and optical axis and the horizontal plane perpendicular to the object plane  $u$ . Then the optical axis makes a  $\gamma$  angle with the normal vector  $\vec{n}$  of object plane  $u$ .  $\gamma$  is called latitude angle and  $\tau = 1/\cos \gamma$  which is called absolute tilt. The latitude angle results in apparent image deformation by resampling the image along the longitudinal direction, and so does the absolute tilt.  $\lambda$  denotes the distance between the camera and object plane along the optical axis, which is the scale factor. And  $\psi$  is induced when the camera rotates around its optical axis. For better illustration, the geometric interpretation is shown in Fig. 3 (b), which shows the affine decomposition between the front view and a slanted view.  $C$  represents the camera image plane and  $O$  is the optical center.

In indoor localization, the affine model can be simplified. Firstly, the rotation angle  $\psi$  can be eliminated as the camera is fixed on the robot. Then as illustrated in [27], there is a transformation relationship between the affine model and rotation matrix of the camera relative to the object. With the rotation matrix denoted as  $R$  and the entry in  $m$  row and  $n$  column as  $R_{mn}$ , the latitude and longitude angle can be expressed as:

$$\gamma = \arccos(R_{33}) \quad (3)$$

$$\phi = |\arctan(R_{31}/R_{32})| \quad (4)$$

In locally planar moving situation, the rotation matrix of the camera can be formulated by one rotation angle, which takes the form as in (1). By setting the coordinate system of the vertical flat object as the coordinate system of camera, and denoting the rotation angle around axis  $y$  as  $\alpha$ , we have

$$\gamma = \arccos(\cos \alpha) = \alpha \quad (5)$$

$$\phi = |\arctan(-\sin \alpha/0)| = \pi/2 \quad (6)$$

Then the affine model in local planar motion is:

$$\mathbf{A} = \lambda \begin{bmatrix} \tau & 0 \\ 0 & 1 \end{bmatrix} \begin{bmatrix} 0 & -1 \\ 1 & 0 \end{bmatrix} \quad (7)$$

where  $\tau = 1/\cos \gamma = 1/\cos \alpha$ .

The above affine model illustrates the deformation between a front view and a slanted view. While in real world applications, the reference image may not be a front view. Therefore, we are going to derive the affine model between two slanted views. The affine model of the two cameras relative to the object plane is as follows:

$$\mathbf{A}_1 = \lambda_1 \begin{bmatrix} \tau_1 & 0 \\ 0 & 1 \end{bmatrix} \begin{bmatrix} 0 & -1 \\ 1 & 0 \end{bmatrix}, \mathbf{A}_2 = \lambda_2 \begin{bmatrix} \tau_2 & 0 \\ 0 & 1 \end{bmatrix} \begin{bmatrix} 0 & -1 \\ 1 & 0 \end{bmatrix} \quad (8)$$

Then the affine model between the two slanted views is

$$\mathbf{A}_{12} = \mathbf{A}_1 \mathbf{A}_2^{-1} = \frac{\lambda_1}{\lambda_2} \begin{bmatrix} \frac{\tau_1}{\tau_2} & 0 \\ 0 & 1 \end{bmatrix} \quad (9)$$

It's obvious that the transition tilt  $\tau_{12} = \tau_1/\tau_2$  and transition rotation  $\phi_{12} = 0$  from the expression of  $\mathbf{A}_{12}$  in (9). Therefore, the resulting transformation is a longitudinal stretch of the image (plus scaling).

**Augmentation strategy:** Lots of feature descriptors are fully scale-invariant such as SIFT [24], SuperPoint [28]. Therefore, we focus only on the tilt invariance strategy which can be then integrated with the scale-invariant descriptors to achieve full affine invariance. To achieve tilt invariance, the query image is augmented by applying all possible transition tilts and the obtained distorted query images are then matched with the reference image. Considering the translation tilt of the two tilted images in real world applications, we sample the tilt  $\tau$  following the geometric series as:  $1, \sqrt{2}, 2, 2\sqrt{2}, 4, 4\sqrt{2}$  to simulate different translation tilts for augmentation [13]. Finally, the feature correspondences obtained by matching all augmented query images are combined together after the inverse tilt operation, and the redundant matches are removed of which the Euclidean distance is less than 1 pixel. As the proposed augmentation-based feature matching algorithm is integrated with the local planar motion property, it is more efficient and effective compared with ASIFT [13].

### C. Minimal solution

In this section, we briefly introduce the minimal solution namely 1P1DP proposed in our previous work [12], which utilizes one point correspondence with depth (DP) and one

point correspondence without depth (P) to solve the camera pose by taking the property into consideration. Specifically, there are three unknown variables in robot pose with local planar motion as shown in (1). According to projection geometry, two constraints about the pose can be derived using one 3D-2D correspondence. And one epipolar constraint can be derived using one 2D-2D correspondence. Then the pose estimation problem of the locally planar moving robot can be solved by combining the three constraints together. More details can be found in [12].

### D. Map selection

In general, a map for visual localization is constructed from a series of sequentially collected frames about the environment. In order to ensure the coverage of the map, the map usually stores observations of dozens or hundreds of map frames, and the capacity of the map will be larger for large scenes. However, with the proposed TiltR2D2 feature matching method which is fully affine invariant, the capacity of the map can be significantly reduced. Specifically, since the proposed method is robust to large viewpoint changes, the map frames can retain only those orthographic views that face the main walls of the room. Then the transition tilt degenerates to the absolute tilt of query view  $\tau_{12} = \tau_1$ , as the reference view is a front view with  $\tau_2 = 1$ . This makes sense because the proposed method makes the map construction process simpler and easier to execute compared to existing methods of acquiring sequential image sequences for map building. And the capacity of the map is substantially reduced for more devices equipped with low computing resources. Subsequent experimental results show that the strategy achieves smaller map storage without affecting localization performance and is suitable for robot platforms with limited computing resources. More details can be found in Appendix-E<sup>1</sup>.

## IV. EXPERIMENTAL RESULTS

For performance validation, we first conduct simulation experiments to evaluate i) the accuracy and robustness of feature matching and the performance in ii) homography estimation and iii) visual localization. And the computing efficiency is also discussed. In real world experiments, we use both public indoor localization dataset and self-collected dataset for validation. The experiments are performed on a desktop with CPU of Intel i7-7700 @ 3.60GHz × 8 and GPU of TITAN X × 4.

### A. Simulation Experiments

In this section, we design an indoor simulation environment in Gazebo to satisfy the local planar motion property.

**Data setup:** The simulation indoor environment is surrounded by four walls, and we randomly select four images from the HPatches dataset [29] as textures to be attached to each of these four walls. A wheeled robot equipped with camera sensors is controlled in the environment for data collection. We first make the robot face the four walls to obtain four map reference images, and then control the robot

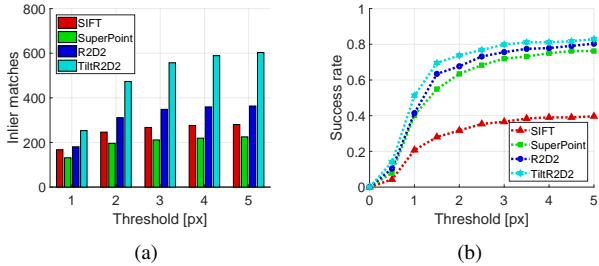


Fig. 4. (a) Comparison of feature matching accuracy. (b) Accuracy of homography estimation.

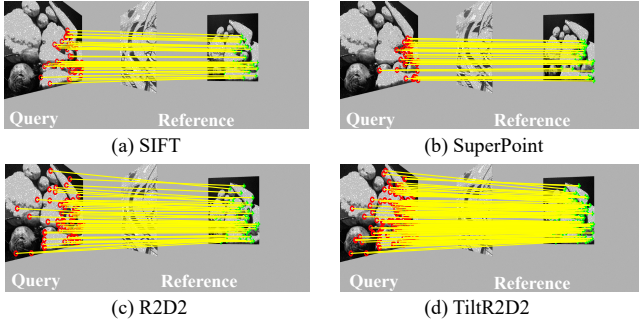


Fig. 5. Matching examples of simulation experiment. The shown matches are inliers with the error less than 1 pixel.

to move randomly in the room to acquire query images. The resolution of the images is  $752 \times 480$  and total of 164 query images are obtained for evaluation.

**Feature matching:** The well-known handcrafted descriptor SIFT [24] and learning-based descriptors SuperPoint [28] and R2D2 [10] are adopted for comparison. As the experimental results in our previous work [12] show that the matching performance of R2D2 is better than the SIFT and SuperPoint, we directly apply tilt augmentation on R2D2, and the obtained method is denoted as TiltR2D2.

We match each query image with all four reference images and then select the one with the most feature matches as the matching result. For evaluation, the ground truth homography matrix between the query image and the reference image is computed using the known camera motion and plane parameters. Then the number of correct feature matches is counted for each image pair under the varying pixel error threshold, as in [13]. The result is shown in Fig. 4 (a). As can be seen from the result, thanks to the effective tilt augmentation strategy, the proposed TiltR2D2 achieves significantly more accurate feature matches at each threshold. Some feature matching cases are shown in Fig. 5 for better illustration.

**Homography estimation:** More accurate feature matching is not equivalent to more accurate geometric estimation, since the distribution of the matches is also essential. Therefore, we next conduct a homography estimation experiment. The corner correctness metric is utilized for evaluation which is computed by comparing the four corners on one image and the transformed corners on another using the estimated homography and the ground truth homography, respectively. The estimated homography is considered to be correct if

the average error of the four corner points is less than a certain threshold. Then we calculate the success rate to quantitatively evaluate the performance of homography estimation, following [28].

For all methods, RANSAC-based robust homography estimation is performed and the result is shown in Fig. 4 (b), from which we can find that the proposed TiltR2D2 achieves higher accuracy among all error thresholds. The results demonstrate that the feature correspondences obtained by the proposed TiltR2D2 can be used to perform the better geometric estimation.

**Localization performance:** In the final, we run the complete visual localization system in the synthetic indoor environment mentioned before. As the plane parameters of each wall are known, the depth of each feature point can be computed by intersecting the projection ray with the plane, such that the 2D-3D correspondences can be obtained. The success rate among different translation error thresholds of different algorithms is shown in Fig. 6 (a), and the rotation error threshold is fixed as 5 degree. For clear demonstration, we only show the estimation results of two solvers: 1P1DP and EPnP, which are tested with different feature matching methods. Results show that the proposed motion property aided localization system can achieve the best performance compared with other methods.

Furthermore, we group the query images according to the viewpoint difference with the reference image and test with EPnP for clear comparison. Results are shown in Fig. 6 (b-d), from which we can find that the advantage of the proposed tilt augmentation feature matching becomes more obvious when the viewpoint difference is larger.

**Runtime:** We count the average computation time per simulation image in feature matching as follows: SIFT (0.08s), SuperPoint (0.04s), R2D2 (0.26s), TiltR2D2 (0.32s). The above performance is obtained by using batch processing technique with one GPU, and the proposed method takes only 1.2 times longer by augmenting 5 images, which meets the real-time requirement. The detailed computational complexity analysis is presented in Appendix-B<sup>1</sup>.

## B. Experiments on OpenLORIS

The OpenLORIS dataset [30] is collected by a wheeled robot equipped with a RealSense D435i. Challenging lifelong changes are presented in the dataset caused by illumination, viewpoint variations, and dynamic objects/human occlusions. And the dataset covers a variety of common scenes in daily life, which is universal and representative for indoor localization testing.

**Data setup:** In OpenLORIS dataset, there are 4 different scenes tested in the paper, including *home*, *office*, *corridor* and *cafe*. For each scene, there are multiple sequences which are collected in different time periods. As in [9], we first downsample each sequence so that the minimum distance between images is 1 m or the minimum angular difference is 20 degree. Then the selected images can meet the requirements of covering a wide range of geographical locations and appearances while being representative enough.

TABLE I  
PERFORMANCE COMPARISON ON DIVIDED OPENLORIS.

Changes	Case Num	Small PC						Large PC						TiltR2D2						SIFT			Superpoint			R2D2			TiltR2D2	
		SIFT			Superpoint			R2D2			TiltR2D2			SIFT			Superpoint			R2D2			TiltR2D2							
		Inlier Num	Suc Rate	Inlier Num	Suc Rate	Inlier Num	Suc Rate	Inlier Num	Suc Rate	Inlier Num	Suc Rate	Inlier Num	Suc Rate	Inlier Num	Suc Rate	Inlier Num	Suc Rate	Inlier Num	Suc Rate	Inlier Num	Suc Rate	Inlier Num	Suc Rate							
Home	Static	68	12.41	0.61	29.60	0.62	84.54	0.78	320.00	<b>0.79</b>	6	1.17	0.17	5.50	0.33	15.83	0.33	65.50	<b>0.50</b>											
	Illumination	35	7.54	0.26	15.97	0.51	15.77	0.63	48.94	<b>0.70</b>	5	2.00	F	1.00	0.40	1.40	0.40	3.60	<b>0.60</b>											
	Man-made	95	7.54	0.19	13.34	0.53	13.89	0.53	46.09	<b>0.55</b>	22	2.09	0.05	3.18	0.09	2.59	0.23	7.91	<b>0.41</b>											
Corridor	Static	312	41.20	0.44	73.99	0.50	129.97	0.71	550.21	<b>0.73</b>	7	1.71	0.14	3.00	0.14	3.00	0.14	17.00	<b>0.29</b>											
	Illumination	151	11.07	0.12	19.72	0.22	26.85	0.19	103.84	<b>0.25</b>	130	0.31	F	0.22	F	0.16	F	0.63	F											
	Man-made	177	20.99	0.25	36.79	0.38	56.45	0.45	194.98	<b>0.45</b>	90	0.46	F	0.42	0.01	0.50	0.01	1.61	<b>0.02</b>											
Office	Static	14	25.64	0.71	62.50	0.93	122.36	<b>1.00</b>	526.85	<b>1.00</b>	-	-	-	-	-	-	-	-	-											
	Illumination	37	13.41	0.22	25.27	0.70	17.43	0.76	52.89	<b>0.89</b>	2	0	F	1.00	F	5.00	F	26.50	<b>0.50</b>											
	Man-made	27	12.00	0.26	24.00	0.59	24.00	0.78	79.41	<b>0.81</b>	19	0.74	F	0.53	F	0.61	0.12	2.11	<b>0.21</b>											
Cafe	Static	38	41.05	0.37	59.37	0.47	125.66	0.45	499.89	<b>0.53</b>	2	15.50	F	8.50	F	22.00	F	73.00	F											
	Illumination	6	20.00	0.50	33.33	0.67	61.33	0.67	203.67	<b>0.67</b>	-	-	-	-	-	-	-	-	-											
	Man-made	8	26.75	0.38	42.25	0.50	59.00	0.50	217.75	<b>0.63</b>	6	2.67	F	5.33	F	3.33	F	9.83	<b>0.33</b>											

<sup>1</sup> F denotes failure localization.

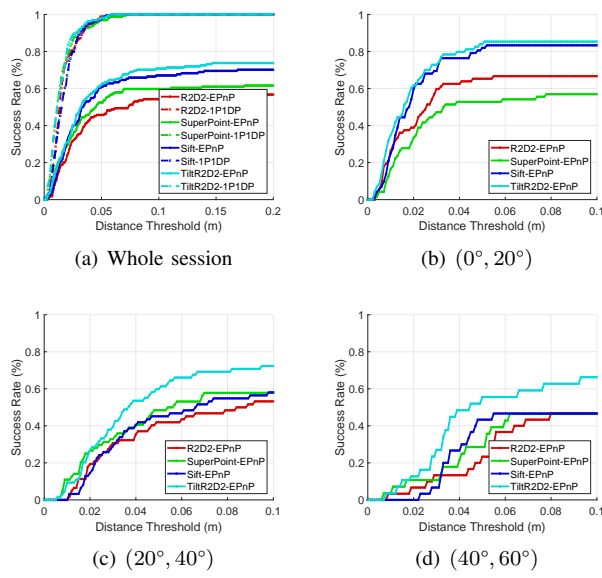


Fig. 6. (a): Localization performance on whole session. (b)-(d): Success rate comparison with increasing viewpoint difference.

The details for generating image pairs for evaluation can be found in Appendix-C<sup>1</sup>.

**Classification protocol:** For each image pair, we extract correspondences using the baseline feature matching method SIFT and then perform two widely used pose estimation algorithms EPnP [11] and P3P [31] in RANSAC [20] for robust estimation. If both of the above methods localize successfully with translation error lower than 0.5 m and rotation error smaller than 5 degree, it indicates that this image pair can be easily matched. And this image pair is excluded as there is no point to exploring in an easy level. If localization fails, according to different PC, we categorize the image pairs into **large PC** category, if the viewpoint difference is larger than 25 degree, otherwise **small PC** category. We further classify the image pairs according to different changes to **static** if the query sequence and the reference sequence are the same one, and **EC** if there is illumination or man-made change, as summarized in Table I.

**Evaluation measures:** We count the average number of correct feature matches as the evaluation metric for *matching accuracy*. Specifically, the ground truth fundamental matrix between the query image and reference image is computed

TABLE II  
SUCCESS RATE COMPARISON ON LOBBY DATASET.

Method	SIFT			SuperPoint			R2D2			TiltR2D2		
	m	0.25/0.50/1.0	0.25/0.50/1.0	0.25/0.50/1.0	deg	5/5/5	5/5/5	5/5/5	5/5/5	5/5/5	5/5/5	5/5/5
P3P	15.22	17.39	19.57	47.83	58.70	63.04	82.61	93.48	93.48	91.30	95.65	95.65
EPnP	4.35	4.35	4.35	43.48	50.00	52.17	76.09	82.61	82.61	80.43	91.30	91.30
AP3P	10.87	13.04	13.04	41.30	50.00	54.35	82.61	91.30	91.30	89.13	93.48	93.48
1P1DP	<b>60.87</b>	<b>67.39</b>	<b>67.39</b>	<b>60.87</b>	<b>78.26</b>	<b>78.26</b>	<b>84.78</b>	<b>93.48</b>	<b>93.48</b>	<b>95.65</b>	<b>97.83</b>	<b>97.83</b>

using the ground truth camera pose and camera parameters. Then we find the correct correspondences that agree with the epipolar geometry between the image pair using Sampson distance as in [32]. We also report the success rate of localization to evaluate *localization robustness*. The details to compute the success rate can be found in Appendix-G<sup>1</sup>.

**Stratified evaluation:** In this section, we perform 1P1DP as the pose estimation algorithm to test the performance of the whole system. Superpoint [28] and R2D2 [10] are selected as representatives of learning-based features which are shown to outperform traditional features and are tested in various real world datasets [12], [33], [34].

From the results in Table I, we can find that the performance of the proposed system outperforms the others in all sequences with all categories, as the more inliers brought by the proposed method significantly promote the localization performance. This enhancement is more obvious in *office-illumination-largePC* and *cafe-man-made-largePC*, where the proposed method breaks through to successful localization when all other methods fail. Comparison of performance in EC and PC are summarized in Fig. 7. Results show that the improvement of the proposed method is significant under large PC, with 67% improvement with pure PC (Static+Large PC category) and even 120% improvement in condition with both EC and large PC. The proposed method also outperforms comparison methods under small PC, with an 8% improvement in condition with pure EC.

In addition, we can find that the improvement of learning-based feature matching is obvious compared to SIFT under small PC, especially in the presence of EC. However, with large PC, the performance of learning-based feature matching is basically no improvement over SIFT. In summary, using the learning-based approach to learn EC under small PC is significantly effective, but solving large PC matching problems by learning is challenging. This is consistent with the results found in [9] and shows that the work in this

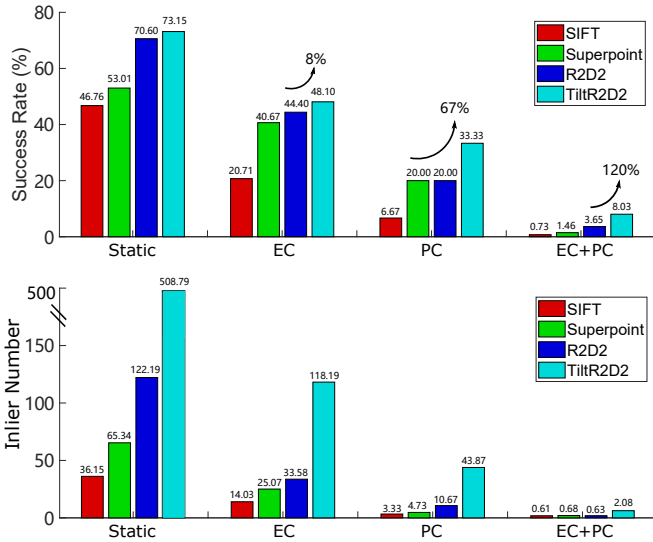


Fig. 7. Performance in dimensions of EC and PC.

paper does a good job of bridging this gap to promote the applications of service robots.

**Full localization system performance:** For complete system evaluation, we also show the localization performance of different solvers including EPnP [11], P3P [31], AP3P [35], and 1P1DP [12], and different feature matching methods on the whole OpenLORIS dataset. Results show that the proposed system achieves the best localization performance on all 12 sessions under all error thresholds, and the detailed success rate comparison can be found in Appendix-D<sup>1</sup>. Furthermore, with the proposed TiltR2D2 used as the front-end, all pose estimation algorithms are improved to different degrees. This enhancement is more apparent in the *cafe* session, where the distance from the robot to the wall is shorter and thus the change in viewpoint is more significant.

### C. Experiments on Lobby

We also test the performance in a self-collected Lobby dataset. The dataset is collected by a mobile robot equipped with five cameras and a 2D LiDAR as shown in Fig. 8 (a). The camera equipped is the BFS-PGE-88S6C-C pointgrey camera with a wide-angle lens with a 6mm focal length. The 2D LiDAR is HOKUYO UTM-30LX. The servo used to rotate the 2D LiDAR is dynamixel mx-64R. More details about the lobby environment can be found in Appendix-H<sup>1</sup>.

**Data setup:** We manually control the robot to move around in the lobby and acquire total 50 images. The resolution of each image is  $1024 \times 540$ . We obtain 3D scans by controlling the servo to rotate the 2D LiDAR for 360 degrees to improve the density of the acquired point cloud. The ground truth camera pose is obtained by aligning the dense synchronized 3D scans. And the 3D points of each image pixel are acquired by projecting the LiDAR scan into the image using the calibrated parameters.

**Localization performance:** We manually select 4 images facing the walls as the reference images as shown in Fig. 8(b) and the remaining 46 images as the query images for eval-

TABLE III  
SUCCESS RATE COMPARISON OF MAP SELECTION EXPERIMENT.

Method	SuperPoint-EPnP	TiltR2D2-EPnP	TiltR2D2-1P1DP
m	0.25 / 0.50 / 1.0	0.25 / 0.50 / 1.0	0.25 / 0.50 / 1.0
deg	5 / 5 / 5	5 / 5 / 5	5 / 5 / 5
Selected 4 - map	36.67 / 43.33 / 46.67	90.00 / 93.33 / 93.33	<b>100.0 / 100.0 / 100.0</b>
Random 4 - map	30.00 / 33.33 / 33.33	56.67 / 63.33 / 63.33	63.33 / 70.00 / 70.00
Random 12 - map	50.00 / 63.33 / 63.33	93.33 / 93.33 / 93.33	96.67 / 100.0 / 100.0
Random 20 - map	63.33 / 70.00 / 70.00	96.67 / 96.67 / 96.67	100.0 / 100.0 / 100.0

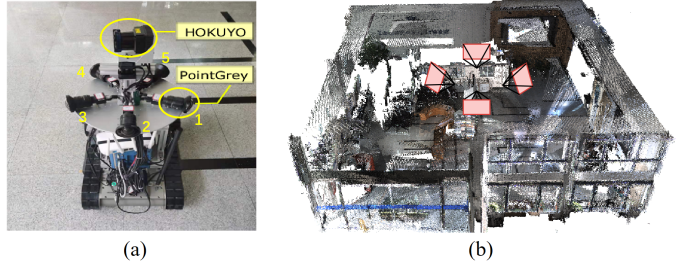


Fig. 8. (a) The platform used to collect Lobby dataset. (b) The reconstructed whole point cloud of the Lobby colored by projected pixels on images. The camera positions to get the selected map frames are shown.

uation. Each query image is matched with these 4 reference images for the subsequent pose estimation. The localization performance is shown in Table II. Results show that the proposed system achieves the best performance, which is consistent with the results in OpenLORIS. Furthermore, the results show that with the help of augmentation-based feature matching, the proposed system gets more robustness against viewpoint variances, such that four reference images facing the walls are sufficient for robust indoor localization.

**Map selection:** In Section III-D, a guide for map frame selection is proposed, which advocates to select a map containing map frames with orthographic views that face the main walls to complete the localization. To demonstrate the effectiveness of the map selection guide, we compare the localization results using maps of varying sizes. To be specific, we first select 30 images as query images and randomly select 4, 8, 12, 16, and 20 images to construct the map among the remaining 20 images. We select the three most representative results on randomly selected map to show in Table III, and the detailed setting of the experiment and the full results can be found in Appendix-E<sup>1</sup>. Results with SuperPoint-EPnP show that the localization performance is enhanced with the increase of map size. However, the results with TiltR2D2-EPnP reflect that the performance on the selected map is similar to that of using 12 reference images and the promotion from a larger map is not significant. With TiltR2D2-1P1DP, the performance of the selected map containing only 4 images is the same as that using 20 images, which validates the effectiveness of the proposed system.

## V. CONCLUSION

In this paper, we propose that the most critical challenge of current indoor localization is perspective change, and construct a dedicated dataset segmentation to verify the hypothesis. To the best of our knowledge, this is the first specific evaluation of the perspective change dimension that can help community to quantitatively understand the

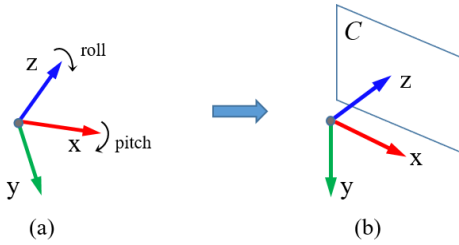


Fig. 9. (a) The original camera coordinate system. (b) The rotated virtual camera coordinate system.

remaining challenges of current indoor localization. Then a complete visual localization system that leverages the local planar motion property is proposed to solve the problem. Experimental results on the public dataset and self-collected dataset demonstrate the effectiveness of the proposed system in challenging long-term indoor localization. In the future, we are going to analyze strategies for eliminating affine distortion in outdoor localization.

## APPENDIX

### A. The details of assumption in planar motion property

Since the camera is not necessarily mounted on the robot with the imaging plane perpendicular to the ground, a virtual camera coordinate system can be constructed such that the y-axis of this coordinate system is perpendicular to the ground, as shown in Fig. 9 (b). The virtual coordinate system can be reached by rotating the original camera coordinate system by certain angles around the x and z axes, and the corresponding rotation angle (i.e. pitch and roll) can be obtained from extrinsic calibration. Therefore, the assumption that the camera plane is perpendicular to the ground can be satisfied.

### B. Computational complexity analysis

The complexity of the TiltR2D2 method is analysed in the recommended configuration: the sampling of tilt follows geometric series as:  $1, \sqrt{2}, 2, 2\sqrt{2}, 4, 4\sqrt{2}$ . And the total computation time of obtaining feature matches consists of two parts, feature extraction and feature matching. Note that the proposed augmentation strategy is only applied on the query image in all experiments, as multiple augmentations of the query image are sufficient to produce a deformation similar to that of the reference image. In addition, if the augmentation of the reference image is required for better performance, it can be performed off-line.

(1) **Feature extraction.** For the first, as the complexity of the sparse feature extraction is proportional to the input image area, estimating the complexity can be attributed to calculating the image area augmented by the proposed strategy. One can verify that the total image area augmented by TiltR2D2 is about 3 times as large as that of the original images, where

$$1 + \frac{1}{\sqrt{2}} + \frac{1}{2} + \frac{1}{2\sqrt{2}} + \frac{1}{4} + \frac{1}{4\sqrt{2}} = 2.9874 \approx 3 \quad (10)$$

Therefore, without any parallel technique, the feature extraction time of TiltR2D2 is 3 times longer than that of

R2D2. In addition, using batch processing techniques, a total of 5 augmented images can be fed into the network along with the original image to generate features through a single propagation. Therefore, the final feature extraction takes about the same time as the original method, and the technique can be implemented with only *one GPU*. Note that even in the case of low resolution under  $3 \times 3$  subsampling factor, the ASIFT method requires 1.5 times the computation time, which shows the advantage of applying motion property to feature extraction of the proposed method.

(2) **Feature matching.** For the second, since the image area for feature extraction is 3 times larger, the number of extracted features is also 3 times larger, resulting in an increase in complexity of feature matching by a factor of about 3. After the experimental statistics, the feature matching time of one image with R2D2 method is about 0.03s. Therefore the feature extraction time plus 3 times the feature matching time results in a final overall time complexity increase of 20%.

(3) **Real application.** Although the proposed TiltR2D2 method is the slowest, it is performed on low frequency keyframes for global localization or loop closure detection tasks. A global localization frequency of nearly 3Hz combined with a high frequency visual odometry can meet the demand for real-time localization in a localization system. In addition, the features for reference images and the augmentation of the reference images can be calculated in advance, which does not add additional time complexity. Therefore, it is a meaningful tradeoff for system performance.

### C. Data setup of divided OpenLORIS

For clearer presentation, we unify the notion of different scenarios in the dataset as “scene”. For example, in OpenLORIS dataset, there are 4 different “scenes” tested in the paper, including *home*, *office*, *corridor* and *cafe*. For each scene, there are multiple “sequences” which are collected in different time periods. For example, in *home* scene, there are 5 sequences including *home1*, *home2*, *home3*, *home4* and *home5*. To generate image pairs for evaluation, we select any two sequences for matching. And one of the two sequences is selected as reference sequence, the other is query sequence. For example, in *home* scene, since there are 5 sequences, there are a total of 10 possible combinations. For each image in the query sequence, a reference image with the highest similarity in the reference sequence is retrieved using the place recognition method NetVLAD. More details can be found in the source code available on <https://github.com/slinkle/Divided-Openloris>.

### D. Localization performance on whole OpenLORIS

For complete system evaluation, we show the localization performance of different solvers and feature matching methods on the whole OpenLORIS dataset. The success rate under different error thresholds is shown in Table IV.

### E. Details of map selection

In general, a map for visual localization is constructed from a series of sequentially collected frames about the

TABLE IV  
SUCCESS RATE COMPARISON ON WHOLE OPENLORIS DATASET.

Task	session m degree	home2 0.25 / 0.5 / 1.0 5 / 5 / 5	home4 0.25 / 0.5 / 1.0 5 / 5 / 5	home5 0.25 / 0.5 / 1.0 5 / 5 / 5	corridor2 0.25 / 0.5 / 1.0 5 / 5 / 5	corridor3 0.25 / 0.5 / 1.0 5 / 5 / 5	corridor4 0.25 / 0.5 / 1.0 5 / 5 / 5
R2D2	P3P	51.67 / 62.84 / 65.14	34.62 / 45.14 / 47.82	64.18 / 65.60 / 65.73	7.85 / 24.07 / 43.63	0.81 / 2.95 / 8.10	8.79 / 17.42 / 24.46
	EPnP	50.93 / 62.27 / 63.94	35.56 / 45.04 / 46.92	68.42 / 69.32 / 69.32	5.81 / 19.31 / 37.97	0.38 / 2.63 / 5.85	7.84 / 15.38 / 21.59
	AP3P	50.33 / 62.47 / 64.88	37.01 / 46.78 / 48.57	67.91 / 68.93 / 68.93	5.87 / 18.84 / 37.91	0.60 / 2.10 / 6.08	7.64 / 15.89 / 21.79
	IP1DP	<b>57.91 / 69.31 / 71.48</b>	<b>47.35 / 61.77 / 65.19</b>	<b>85.88 / 86.91 / 86.91</b>	<b>11.30 / 31.09 / 50.85</b>	<b>1.76 / 5.91 / 13.96</b>	<b>13.87 / 26.63 / 31.87</b>
TiltR2D2	P3P	52.90 / 66.74 / 69.55	37.11 / 49.18 / 52.14	64.06 / 65.60 / 65.73	10.04 / 27.61 / 44.26	1.19 / 4.29 / 9.48	15.14 / 21.23 / 24.83
	EPnP	51.80 / 64.51 / 67.21	36.36 / 46.92 / 49.55	69.51 / 70.31 / 70.31	10.58 / 27.64 / 43.63	0.81 / 3.33 / 7.86	15.30 / 19.38 / 21.97
	AP3P	52.77 / 66.64 / 69.38	36.40 / 49.04 / 52.14	69.46 / 71.26 / 71.26	10.01 / 27.41 / 43.80	1.19 / 4.10 / 9.29	14.88 / 20.86 / 24.35
	IP1DP	<b>60.34 / 72.11 / 74.28</b>	<b>49.98 / 62.66 / 68.15</b>	<b>87.03 / 87.80 / 87.80</b>	<b>15.59 / 35.17 / 52.98</b>	<b>1.76 / 7.19 / 16.39</b>	<b>18.32 / 26.79 / 31.97</b>
Task	session m degree	corridor5 0.25 / 0.5 / 1.0 5 / 5 / 5	office3 0.25 / 0.5 / 1.0 5 / 5 / 5	office4 0.25 / 0.5 / 1.0 5 / 5 / 5	office5 0.25 / 0.5 / 1.0 5 / 5 / 5	office7 0.25 / 0.5 / 1.0 5 / 5 / 5	cafe1 0.25 / 0.5 / 1.0 5 / 5 / 5
R2D2	P3P	29.97 / 50.25 / 68.43	56.11 / 56.11 / 56.11	70.92 / 71.15 / 71.15	81.94 / 83.51 / 83.51	87.03 / 88.96 / 88.96	30.50 / 62.06 / 80.15
	EPnP	30.08 / 50.59 / 69.92	55.56 / 55.56 / 55.56	71.15 / 71.61 / 71.61	81.18 / 82.82 / 82.88	87.03 / 88.87 / 88.87	31.79 / 62.65 / 80.68
	AP3P	29.88 / 50.39 / 69.19	56.11 / 56.11 / 56.11	70.92 / 71.15 / 71.26	81.91 / 83.53 / 83.53	83.70 / 85.49 / 85.49	30.21 / 62.47 / 79.98
	IP1DP	<b>34.70 / 56.69 / 74.69</b>	<b>58.33 / 58.61 / 58.61</b>	<b>74.14 / 76.44 / 76.44</b>	<b>89.36 / 90.25 / 90.25</b>	<b>90.97 / 92.11 / 92.11</b>	<b>39.99 / 72.54 / 82.32</b>
TiltR2D2	P3P	37.37 / 55.46 / 74.01	56.11 / 56.11 / 56.11	71.15 / 71.26 / 71.38	84.33 / 85.97 / 85.97	87.20 / 88.96 / 88.96	49.06 / 76.93 / 85.19
	EPnP	36.93 / 56.21 / 73.92	56.39 / 56.39 / 56.39	71.15 / 71.61 / 71.72	82.50 / 83.53 / 83.53	87.03 / 89.13 / 89.13	50.06 / 78.04 / 85.19
	AP3P	37.25 / 55.39 / 73.76	56.39 / 56.67 / 56.67	71.03 / 71.15 / 71.26	83.64 / 85.34 / 85.34	87.64 / 89.40 / 89.40	48.65 / 76.70 / 85.19
	IP1DP	<b>42.17 / 61.03 / 79.83</b>	<b>58.78 / 58.89 / 59.17</b>	<b>74.71 / 76.67 / 77.24</b>	<b>90.12 / 91.50 / 91.50</b>	<b>91.24 / 92.55 / 92.55</b>	<b>54.22 / 81.03 / 85.66</b>

<sup>1</sup> Considering the map coverage of the environment, the map sequences for each session are as follows: home1 and home3, corridor1, office1 and office2, cafe2.

<sup>2</sup> For testing on office6, all methods achieve 100 success rate over three thresholds.

environment. In order to ensure the coverage of the map, the map usually stores observations of dozens or hundreds of map frames, and the capacity of the map will be larger for large scenes. However, with the proposed TiltR2D2 feature matching method which is fully affine invariant, the capacity of the map can be significantly reduced. Specifically, since the proposed method is robust to large viewpoint changes, the map frames can retain only those orthographic views that face the main walls of the room. For example, for a room enclosed by four walls, a map consisting of only four map frames is required to satisfy the subsequent robust localization. In real applications, for scenarios where a map consists of sequential frames has already been constructed, the “map frame selection guide” expressed in the original manuscript allows you to keep only the map frames facing the main walls to form the selected map. When using this selected map for online localization, the loading and calculation process can be accelerated which is friendly to on-board computing resources. For scenarios where maps have not yet been constructed, this guide simplifies the map construction steps and greatly facilitates map acquisition and construction.

To further demonstrate that the proposed localization system helps to achieve smaller map construction, we show the results with the different number of map images. To be specific, we first select 30 images as query images and randomly select 4, 8, 12, 16, and 20 images to construct the map among the remaining 20 images. Then the localization results are compared with that of the selected map which consists of four images facing walls. When testing on different maps, we choose the top 4 reference images with the highest number of feature matches for pose estimation. The results of all randomly selected map are shown in Table. V.

TABLE V  
SUCCESS RATE COMPARISON OF MAP SELECTION TEST.

Method	SuperPoint-EPnP 0.25 / 0.50 / 1.0 5 / 5 / 5	TiltR2D2-EPnP 0.25 / 0.50 / 1.0 5 / 5 / 5	TiltR2D2-IP1DP 0.25 / 0.50 / 1.0 5 / 5 / 5
Selected 4 - map	36.67 / 43.33 / 46.67	90.00 / 93.33 / 93.33	<b>100.0 / 100.0 / 100.0</b>
Random 4 - map	30.00 / 33.33 / 33.33	56.67 / 63.33 / 63.33	63.33 / 70.00 / 70.00
Random 8 - map	43.33 / 43.33 / 43.33	76.67 / 76.67 / 76.67	83.33 / 86.67 / 90.00
Random 12 - map	50.00 / 63.33 / 63.33	93.33 / 93.33 / 93.33	96.67 / 100.0 / 100.0
Random 16 - map	60.00 / 60.00 / 60.00	96.67 / 96.67 / 96.67	100.0 / 100.0 / 100.0
Random 20 - map	63.33 / 70.00 / 70.00	96.67 / 96.67 / 96.67	100.0 / 100.0 / 100.0

#### F. Discussion on practical applications

There are some additional points to make the practical applications of the proposed localization system more clear.

First of all, the proposed localization system is indeed mainly oriented to applications in indoor environments, but the application scenarios in indoor environments are very extensive, and there is also an urgent need for accurate and robust localization, such as restaurant delivery robots, bank consultation robots, gymnasium security robots, hotel greeting service robots, etc. In addition, the proposed method does not have additional or more strict requirements for the application and can be applied to all common indoor environments, as detailed in the (1)-(3) points below. Furthermore, we validate the proposed system in the outdoor environment using the public outdoor dataset Kaist [36] shown in point (4). The results show that while the proposed approach is theoretically designed for indoor application scenarios, it is also applicable to autonomous driving applications operating on flat roads surrounded by buildings, as shown in the Kaist dataset. The detailed expressions are as follows.

(1) Regarding planar motion, the application scenario of the proposed localization system actually only needs to satisfy the requirements of the locally planar surfaces and does not require a strict globally planar surface. With the aid

of the place recognition method such as NetVLAD [15], the localization range has been narrowed down to a local range within the same scene. For example, in the “home” scene, it is already possible to locate whether the current robot is in the bedroom or the living room. Therefore, as long as the planar requirements are satisfied inside the bedroom, it is not necessary that both the kitchen and the living room are on the same plane. This further expands the application scenario of the proposed system, since many indoor environments are designed with rooms of different heights.

(2) Regarding textured planes, firstly, feature matching methods based on keypoints all require the environment to have texture information, which is a common requirement. Secondly, for the plane requirement, it is easy to satisfy in real indoor environments, as can be seen from the real world experiments in Section IV-B on publicly available OpenLORIS datasets. The test data in all scenes including “home”, “corridor”, “office” and “cafe” are collected in the real indoor environment, and the experimental results verified the feasibility of the proposed method.

(3) A sensitivity experiment is further conducted to test the performance of the proposed method regarding noise on the reduced degree of freedom (DoF), including pitch, roll and  $t_y$ , since noise is unavoidable in real world. In the proposed robust visual localization system, the feature matching at front-end is formulated as a 3DoF problem using the locally planar motion property, while the pose estimation at back-end is actually performed in 6DoF, as the performed 6DoF nonlinear optimization corrects for errors on the reduced 3DoF. Therefore, the sensitivity experiment is conducted on the proposed augmentation-based feature matching method as follows.

Referring to the data setup in the simulation experiment in Section IV-A, we replace the flat ground in the simulation room with a sandy ground with random undulations to generate noise in pitch, roll and  $t_y$  with robot motion. Other experimental settings are the same as in Section IV-A and we collect total 935 query images with varying noise in  $[0, 30]$  degree on both pitch and roll angles and  $[0, 0.05]$  m on  $t_y$ . As in **Homography estimation** experiment in Section IV-A, the corner correctness metric is utilized for evaluation and the average error of the four corner points is shown in Fig. 10 to show the sensitivity performance of the proposed TiltR2D2 method. The results of 6DoF feature matching method SuperPoint and R2D2, whose performance is unaffected by the noise on pitch, roll and  $t_y$  are also shown for comparison. Results show that the improvement in feature matching performance brought by the proposed augmentation strategy can tolerate a large amount of noise, because the performance improvement brought by the proposed method is still significant when the noise increases. In fact, the increase of noise on pitch and roll angles and  $t_y$  directly affects the viewpoint of the acquired image, thus increasing the view angle difference between the query image and the reference image, and the matching performance of the 6DoF method is also affected with the increase of noise. Although the performance of the proposed method also decreases when

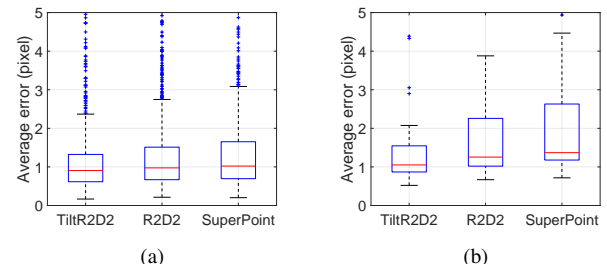


Fig. 10. (a) The noise on  $t_y$  is varying in  $[0, 0.02]$  m. (b) The noise on  $t_y$  is varying in  $[0.02, 0.05]$  m. And the noise on both pitch and roll angles is varying between  $[0, 30]$  degree in (a) and (b).

TABLE VI  
SUCCESS RATE COMPARISON ON KAIST DATASET (%).

	SIFT	SuperPoint	R2D2	TiltR2D2
0.25m/5deg	0.1912	0.2717	2.1526	<b>2.3434</b>
0.50m/5deg	3.0593	3.8152	5.4795	<b>6.6245</b>
1.00m/5deg	10.5163	14.6196	25.8317	<b>28.3202</b>

the noise increases, the performance improvement is still significant compared to other 6DoF methods, which can be explained by the robustness of the viewpoint change brought by the proposed augmentation-based strategy.

(4) In addition, we conduct outdoor environmental experiments, using the public dataset Kaist for testing, which is collected with ground vehicles operating in urban areas. As can be seen from the scenes shown in Fig. 11, the dataset is also consistent with the application of the proposed system, since the motion of the vehicle is also locally planar, while most of the feature points are distributed on buildings with vertical planes. Such a scenario is satisfied in most driverless applications in urban environments. Specific experimental details are given below.

In the dataset, there are two sequences, Urban38 and Urban39. The Urban38 sequence is selected to build the map and Urban39 is used to test the localization performance. The 3D map points are triangulated across multiple adjacent images and the corresponding poses. For each query image, the matched reference image is retrieved using place recognition algorithm NetVLAD. Since the main contribution of the paper is the feature matching method at front-end, we fix the pose estimation algorithm at back-end as 1P1DP-based RANSAC and vary different methods at front-end including: SIFT, SuperPoint, R2D2 and the proposed TiltR2D2. For evaluation, the success rate under different thresholds are computed to evaluate the robustness of different feature matching methods. The results are shown in Table. VI.

As can be seen from the examples in Fig. 11, the viewpoint change between query and reference images is small due to the lane line constraint on the trajectory of the vehicle, and only in a few turning scenes does a large viewpoint change occur. However, the proposed method which uses an augmentation strategy to provide more feature matches still shows some improvement in localization robustness, which verifies the feasibility of the proposed method in

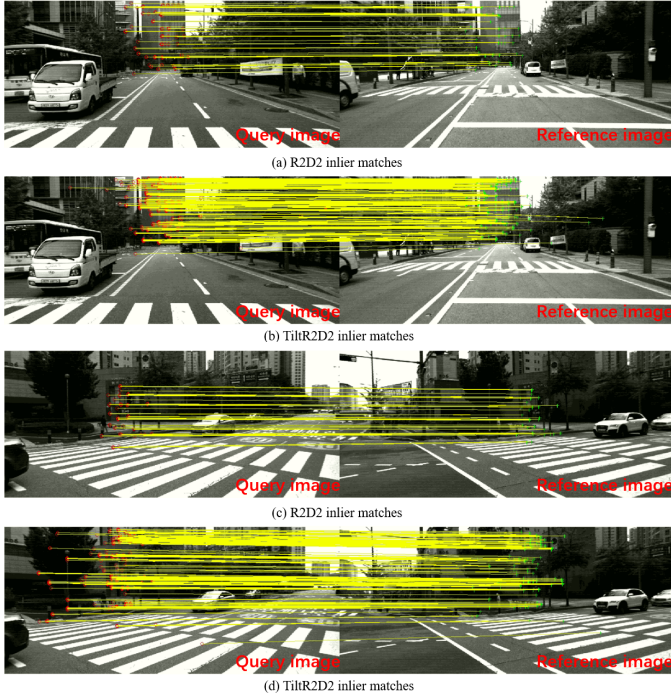


Fig. 11. Some examples in Kaist outdoor dataset. The viewpoint change between query and reference images is small due to the lane line constraint on the trajectory of the vehicle, and only in a few turning scenes does a large viewpoint change occur.

outdoor unmanned application scenarios. Considering that the viewpoint change in the unmanned application scenario is not as severe as that in the indoor scenario, and that the proposed method brings performance improvement at the cost of consuming longer feature extraction time, it is more beneficial to use the proposed method in the indoor application scenario.

#### G. Details about evaluation measures for OpenLORIS

We count the average number of correct feature matches as the evaluation metric for *matching accuracy*. Specifically, the ground truth fundamental matrix between the query image and reference image is computed using the ground truth camera pose and camera parameters. Then we find the correct correspondences that agree with the epipolar geometry between the image pair using Sampson distance as in [32]. We also report the success rate of localization to evaluate *localization robustness*. To get an accurate depth value for each matched feature point, we triangulate scene points using observation from multiple frames and refine the reconstruction with bundle adjustment. Then the translation error of the estimated relative pose and ground truth pose is computed as the Euclidean distance in meter. The rotation error is computed as  $\arccos(0.5Tr(\mathbf{R}\mathbf{R}_{gt}^T) - 0.5)$  in degree, where  $\mathbf{R}_{gt}$  denotes the ground truth relative rotation matrix and  $R$  denotes the estimated one. The localization is successful if the translation error is lower than 0.5 m and rotation error is smaller than 5 degree as in [7].

#### H. Details about Lobby dataset

The Lobby dataset is collected by a mobile robot equipped with five pointgrey cameras and a 2D LiDAR as shown in Fig. 8 (a). The camera equipped is the BFS-PGE-88S6C-C pointgrey camera with a wide-angle lens with a 6mm focal length, not a fisheye lens. The 2D LiDAR is HOKUYO UTM-30LX. The servo used to rotate the 2D LiDAR is dynamixel mx-64R. The Lobby is a  $11m \times 11m$  square with two walls made up of large French windows, so the environment is subject to significant changes in external lighting during the day and artificial lighting at night. The static obstacles in the environment mainly include some tables, chairs and posters, while the dynamic obstacles are the moving pedestrians. The data in the Lobby dataset contains environmental changes from afternoon to evening.

#### REFERENCES

- [1] Z. Chen, J. Guo, X. Xu, Y. Wang, H. Huang, Y. Wang, and R. Xiong, “Pregan: Pose randomization and estimation for weakly paired image style translation,” *IEEE Robotics and Automation Letters*, vol. 6, no. 2, pp. 2209–2216, 2021.
- [2] S. Garg, B. Harwood, G. Anand, and M. Milford, “Delta descriptors: Change-based place representation for robust visual localization,” *IEEE Robotics and Automation Letters*, vol. 5, no. 4, pp. 5120–5127, 2020.
- [3] L. Tang, Y. Wang, X. Ding, H. Yin, R. Xiong, and S. Huang, “Topological local-metric framework for mobile robots navigation: a long term perspective,” *Autonomous Robots*, vol. 43, no. 1, pp. 197–211, 2019.
- [4] X. Ding, Y. Wang, R. Xiong, D. Li, L. Tang, H. Yin, and L. Zhao, “Persistent stereo visual localization on cross-modal invariant map,” *IEEE Transactions on Intelligent Transportation Systems*, 2019.
- [5] P.-E. Sarlin, C. Cadena, R. Siegwart, and M. Dymczyk, “From coarse to fine: Robust hierarchical localization at large scale,” in *Proceedings of the IEEE/CVF Conference on Computer Vision and Pattern Recognition*, 2019, pp. 12716–12725.
- [6] T. Sattler, W. Maddern, C. Toft, A. Torii, L. Hammarstrand, E. Stenborg, D. Safari, M. Okutomi, M. Pollefeys, J. Sivic, et al., “Benchmarking 6dof outdoor visual localization in changing conditions,” in *Proceedings of the IEEE Conference on Computer Vision and Pattern Recognition*, 2018, pp. 8601–8610.
- [7] Y. Jiao, Y. Wang, X. Ding, B. Fu, S. Huang, and R. Xiong, “2-entity ransac for robust visual localization: Framework, methods and verifications,” *IEEE Transactions on Industrial Electronics*, 2020.
- [8] C. Chen, B. Wang, C. X. Lu, N. Trigoni, and A. Markham, “A survey on deep learning for localization and mapping: Towards the age of spatial machine intelligence,” *arXiv preprint arXiv:2006.12567*, 2020.
- [9] A. Jafarzadeh, M. L. Antequera, P. Gargallo, Y. Kuang, C. Toft, F. Kahl, and T. Sattler, “Crowddriven: A new challenging dataset for outdoor visual localization,” in *Proceedings of the IEEE/CVF International Conference on Computer Vision*, 2021, pp. 9845–9855.
- [10] J. Revaud, P. Weinzaepfel, C. De Souza, N. Pion, G. Csurka, Y. Cabon, and M. Humenberger, “R2d2: repeatable and reliable detector and descriptor,” in *Conference on Neural Information Processing Systems (NeurIPS)*, 2019.
- [11] V. Lepetit, F. Moreno-Noguer, and P. Fua, “Epnp: An accurate o (n) solution to the pnp problem,” *International journal of computer vision*, vol. 81, no. 2, p. 155, 2009.
- [12] Y. Jiao, L. Liu, B. Fu, X. Ding, M. Wang, Y. Wang, and R. Xiong, “Robust localization for planar moving robot in changing environment: A perspective on density of correspondence and depth,” in *2021 IEEE International Conference on Robotics and Automation (ICRA)*. IEEE, 2021, pp. 4006–4012.
- [13] J.-M. Morel and G. Yu, “Asift: A new framework for fully affine invariant image comparison,” *SIAM journal on imaging sciences*, vol. 2, no. 2, pp. 438–469, 2009.
- [14] D. Gálvez-López and J. D. Tardos, “Bags of binary words for fast place recognition in image sequences,” *IEEE Transactions on Robotics*, vol. 28, no. 5, pp. 1188–1197, 2012.

- [15] R. Arandjelovic, P. Gronat, A. Torii, T. Pajdla, and J. Sivic, "Netvlad: Cnn architecture for weakly supervised place recognition," in *Proceedings of the IEEE conference on computer vision and pattern recognition*, 2016, pp. 5297–5307.
- [16] S. Lynen, T. Sattler, M. Bosse, J. A. Hesch, M. Pollefeys, and R. Siegwart, "Get out of my lab: Large-scale, real-time visual-inertial localization," in *Robotics: Science and Systems*, vol. 1, 2015.
- [17] T. Sattler, M. Havlena, F. Radenovic, K. Schindler, and M. Pollefeys, "Hyperpoints and fine vocabularies for large-scale location recognition," in *Proceedings of the IEEE International Conference on Computer Vision*, 2015, pp. 2102–2110.
- [18] J. L. Schönberger, M. Pollefeys, A. Geiger, and T. Sattler, "Semantic visual localization," in *Proceedings of the IEEE conference on computer vision and pattern recognition*, 2018, pp. 6896–6906.
- [19] C. Toft, E. Stenborg, L. Hammarstrand, L. Brynte, M. Pollefeys, T. Sattler, and F. Kahl, "Semantic match consistency for long-term visual localization," in *Proceedings of the European Conference on Computer Vision (ECCV)*, 2018, pp. 383–399.
- [20] M. A. Fischler and R. C. Bolles, "Random sample consensus: a paradigm for model fitting with applications to image analysis and automated cartography," *Communications of the ACM*, vol. 24, no. 6, pp. 381–395, 1981.
- [21] Z. Kukelova, M. Bujnak, and T. Pajdla, "Closed-form solutions to minimal absolute pose problems with known vertical direction," in *Asian Conference on Computer Vision*. Springer, 2010, pp. 216–229.
- [22] B. Guan, J. Zhao, Z. Li, F. Sun, and F. Fraundorfer, "Minimal solutions for relative pose with a single affine correspondence," in *Proceedings of the IEEE/CVF Conference on Computer Vision and Pattern Recognition*, 2020, pp. 1929–1938.
- [23] P. Speciale, D. Pani Paudel, M. R. Oswald, T. Kroeger, L. Van Gool, and M. Pollefeys, "Consensus maximization with linear matrix inequality constraints," in *Proceedings of the IEEE Conference on Computer Vision and Pattern Recognition*, 2017, pp. 4941–4949.
- [24] D. G. Lowe, "Distinctive image features from scale-invariant keypoints," *International journal of computer vision*, vol. 60, no. 2, pp. 91–110, 2004.
- [25] E. Rublee, V. Rabaud, K. Konolige, and G. Bradski, "Orb: An efficient alternative to sift or surf," in *2011 International conference on computer vision*. Ieee, 2011, pp. 2564–2571.
- [26] I. Rocco, M. Cimpoi, R. Arandjelovic, A. Torii, T. Pajdla, and J. Sivic, "Ncnet: Neighbourhood consensus networks for estimating image correspondences," *IEEE Transactions on Pattern Analysis and Machine Intelligence*, 2020.
- [27] Q. Wang, W. Zhang, X. Liu, Z. Zhang, M. H. A. Baig, G. Wang, L. He, and T. Cui, "Line matching of wide baseline images in an affine projection space," *International Journal of Remote Sensing*, vol. 41, no. 2, pp. 632–654, 2020.
- [28] D. DeTone, T. Malisiewicz, and A. Rabinovich, "Superpoint: Self-supervised interest point detection and description," in *Proceedings of the IEEE conference on computer vision and pattern recognition workshops*, 2018, pp. 224–236.
- [29] V. Balntas, K. Lenc, A. Vedaldi, and K. Mikolajczyk, "Hpatches: A benchmark and evaluation of handcrafted and learned local descriptors," in *Proceedings of the IEEE conference on computer vision and pattern recognition*, 2017, pp. 5173–5182.
- [30] X. Shi, D. Li, P. Zhao, Q. Tian, Y. Tian, Q. Long, C. Zhu, J. Song, F. Qiao, L. Song, et al., "Are we ready for service robots? the openloris-scene datasets for lifelong slam," in *2020 IEEE International Conference on Robotics and Automation (ICRA)*. IEEE, 2020, pp. 3139–3145.
- [31] X.-S. Gao, X.-R. Hou, J. Tang, and H.-F. Cheng, "Complete solution classification for the perspective-three-point problem," *IEEE transactions on pattern analysis and machine intelligence*, vol. 25, no. 8, pp. 930–943, 2003.
- [32] Q. Zhou, T. Sattler, and L. Leal-Taixe, "Patch2pix: Epipolar-guided pixel-level correspondences," in *Proceedings of the IEEE/CVF conference on computer vision and pattern recognition*, 2021, pp. 4669–4678.
- [33] P.-E. Sarlin, D. DeTone, T. Malisiewicz, and A. Rabinovich, "Superglue: Learning feature matching with graph neural networks," in *Proceedings of the IEEE/CVF conference on computer vision and pattern recognition*, 2020, pp. 4938–4947.
- [34] J. Ma, X. Jiang, A. Fan, J. Jiang, and J. Yan, "Image matching from handcrafted to deep features: A survey," *International Journal of Computer Vision*, vol. 129, no. 1, pp. 23–79, 2021.
- [35] T. Ke and S. I. Roumeliotis, "An efficient algebraic solution to the perspective-three-point problem," in *Proceedings of the IEEE Conference on Computer Vision and Pattern Recognition*, 2017, pp. 7225–7233.
- [36] J. Jeong, Y. Cho, Y.-S. Shin, H. Roh, and A. Kim, "Complex urban dataset with multi-level sensors from highly diverse urban environments," *The International Journal of Robotics Research*, vol. 38, no. 6, pp. 642–657, 2019.